

A learning model for battery lifetime prediction of LoRa sensors in additive manufacturing

Alberto Morato¹, Tommaso Fedullo^{2,3}, Stefano Vitturi¹, Luigi Rovati², Federico Tramarin²

¹ National Research Council of Italy, IEIIT-CNR, Padova, Italy

² Department of Engineering "Enzo Ferrari", University of Modena and Reggio Emilia, Modena, Italy

³ Department of Management and Engineering, University of Padova, Italy

ABSTRACT

Today, an innovative leap for wireless sensor networks, leading to the realization of novel and intelligent industrial measurement systems, is represented by the requirements arising from the Industry 4.0 and Industrial Internet of Things (IIoT) paradigms. In fact, unprecedented challenges to measurement capabilities are being faced, with the ever-increasing need to collect reliable yet accurate data from mobile, battery-powered nodes over potentially large areas. Therefore, optimizing energy consumption and predicting battery life are key issues that need to be accurately addressed in such IIoT-based measurement systems. This is the case for the additive manufacturing application considered in this work, where smart battery-powered sensors embedded in manufactured artifacts need to reliably transmit their measured data to better control production and final use, despite being physically inaccessible. A Low Power Wide Area Network (LPWAN), and in particular LoRaWAN (Long Range WAN), represents a promising solution to ensure sensor connectivity in the aforementioned scenario, being optimized to minimize energy consumption while guaranteeing long-range operation and low-cost deployment. In the presented application, LoRa equipped sensors are embedded in artifacts to monitor a set of meaningful parameters throughout their lifetime. In this context, once the sensors are embedded, they are inaccessible, and their only power source is the originally installed battery. Therefore, in this paper, the battery lifetime prediction and estimation problems are thoroughly investigated. For this purpose, an innovative model based on an Artificial Neural Network (ANN) is proposed, developed starting from the discharge curve of lithium-thionyl chloride batteries used in the additive manufacturing application. The results of experimental campaigns carried out on real sensors were compared with those of the model and used to tune it appropriately. The results obtained are encouraging and pave the way for interesting future developments.

Section: RESEARCH PAPER

Keywords: LoRa; LoRaWAN; IIoT; battery lifetime; machine learning

Citation: Alberto Morato, Tommaso Fedullo, Stefano Vitturi, Luigi Rovati, Federico Tramarin, A learning model for battery lifetime prediction of LoRa sensors in additive manufacturing, Acta IMEKO, vol. 12, no. 1, article 24, March 2023, identifier: IMEKO-ACTA-12 (2023)-01-24

Section Editor: Francesco Lamonaca, University of Calabria, Italy

Received November 17, 2022; **In final form** February 15, 2023; **Published** March 2023

Copyright: This is an open-access article distributed under the terms of the Creative Commons Attribution 3.0 License, which permits unrestricted use, distribution, and reproduction in any medium, provided the original author and source are credited.

Corresponding author: Federico Tramarin, e-mail: federico.tramarin@unimore.it

1. INTRODUCTION

Today, novel and intelligent measurement systems are increasingly developed thanks to the Internet of Things (IoT) paradigm [1]. Moreover, the combination of IoT with the Industry 4.0 [2], [3] paradigm (often referred to as Industrial IoT), introduces a number of unprecedented challenges to measurement capabilities [4], with the ever-increasing need to collect reliable yet accurate data from mobile, battery-powered nodes over potentially large areas. In this scenario, one of the enabling technologies of Industry 4.0 is Additive Manufacturing (AM). Basically, AM makes it possible to create 3D objects, such

as prototypes of possible products designed with CAD tools, without the burdens usually imposed by traditional production systems in terms of work organization, delivery times and material utilization. This has a tremendous impact on manufacturing processes, making them more efficient, timely, scalable, and customizable [5], [6].

The benefits resulting from the introduction of AM also place unprecedented demands on sensor systems and related measurement techniques. In fact, there are several AM applications, such as those based on powder-bed processes, where suitable sensor systems need to be developed to collect data during the manufacturing process of potentially large objects, e.g., for early detection of defects and anomalies, and for

process qualification [7]. This is the case addressed in this paper, where a large powder-bed 3D printer is capable of producing different types of artifacts using mixtures of powders, derived from recycled materials or natural components such as sand, water and chemical-free reagents [8]. A peculiarity of the system is that the artifacts are permanently equipped with sensors. These sensors are embedded in the manufactured objects at the beginning of the production phase and cannot be physically accessed. The sensors are needed to provide measurements of appropriate variables, such as temperature and humidity, which are used for two main purposes: i) during artifact production, as mentioned above, they provide feedback that allows on-line tuning of the 3D printing process and assist in defect detection [9]; ii) during the artifacts' lifetime, when they are in their final positions, sensor data is collected to perform off-line analysis as well as to monitor environmental conditions. A system with these specifications has been developed as part of an Italian regional project called ADMIN-4D (ADditive Manufacturing & INdustry 4.0 as innovation Driver).

Of course, to achieve the above goals, the sensors must also be able to communicate and send the measured data to the correct destination(s). For this purpose, technologies such as Low Power Wide Area Networks (LPWANs) represent a promising solution to ensure sensor connectivity, as they are optimized to minimize energy consumption while ensuring long-range operation and low-cost deployment. In the application addressed in this paper, one of the most representative implementations was chosen, namely LoRaWAN (Long Range WAN) [10], [11]. It is worth noting that the application of LoRaWAN in the industrial scenario has been extensively analyzed [12], [13], proving its effectiveness, possibly after a suitable protocol optimization.

Therefore, the targeted AM application poses several challenges to the sensor network system, and three main issues must be evaluated for the efficient collection of measurement data: i) the effective acquisition of readings from sensors embedded in artifacts; ii) the transmission range of the sensors; iii) the lifetime of the batteries used by the sensors. We have already investigated both the actual transmission capability of the embedded sensors and the covered distances in our previous work [14]. The results are satisfactory. It was found that transmission ranges of several tens of meters could be effectively achieved with a low packet loss rate and under different environmental conditions, in line with the requirements.

In this paper, we deal extensively with the latter issue, namely battery life. Obviously, this is a critical aspect for the whole project, since once an artifact has been produced, its embedded sensors can no longer be accessed, nor can its batteries be replaced/recharged. Consequently, once the lifetime of the batteries has expired, measurements from the sensors will no longer be transmitted. It should also be noted that battery lifetime prediction is of paramount importance in several other IIoT-based applications, such as cooperative robotics [15], [16]. Battery lifetime prediction is closely related to the battery discharge model. Unfortunately, the definition of an analytical discharge model, although theoretically possible, is difficult to achieve from the data typically provided by the manufacturers.

Therefore, in this paper we present a novel approach to battery discharge modeling based on a hybrid scheme where a static model and a machine learning (ML) one coexist. In particular, we use an artificial neural network (ANN), which is necessary to overcome the nonlinearity of battery capacity as a function of temperature, and which is trained and validated using

data derived from the battery datasheet. This ANN model is then used in conjunction with a closed-form static battery model (e.g., an accurately adapted version of the Matlab model) and finally introduced in the context of the AM application described. The ultimate goal is to develop a model that can accurately predict the battery life of sensors under various operating conditions, including changes in temperature, power consumption, and other variables. The model should also be able to account for any nonlinearities that may occur, such as the effect of extreme temperatures on battery performance.

Experimental campaigns were conducted to compare the predictions of the models with real battery data. The models were then configured to emulate typical operating conditions to achieve realistic battery life predictions. As a result, it will be possible to more accurately predict sensor lifetime and optimize communication parameters to ensure maximum battery life.

The paper is organized as follows. Section 2 gives a brief description of the targeted AM application and of the ADMIN-4D project and outlines the requirements for sensor data acquisition. Section 3 discusses some relevant related works and provides an overview of the contributions provided by this paper. Section 4 introduces the adopted sensors and reports considerations about battery selection and characterization. Section 5 describes the adopted dynamic battery discharge model and its tuning, whereas Section 6 presents the developed data-driven discharge model. Section 7 then presents the outcomes of experimental assessments and compares them with the model results. Section 8 presents battery life predictions in the operational context of ADMIN-4D. Finally, Section 9 concludes the paper with some considerations for future developments.

2. THE ADMIN-4D PROJECT

The structure of the ADMIN-4D project is shown in Figure 1. Its operation is characterized by two distinct phases, namely production and final deployment. The production phase, in which an artifact is created, takes a variable amount of time, depending mainly on the size of the artifact itself. Typical production times can be tens of hours. During this phase, sensors are embedded in the artifact and immediately begin transmitting data that is collected by the 3D printer's automation system and used for online feedback. As discussed in the previous Section, the system uses a sensor network based on LoRaWAN. Specifically, a LoRaWAN Gateway (GW) device is connected to the 3D printer's automation system via the ADMIN-4D intranet and provides connectivity to the embedded

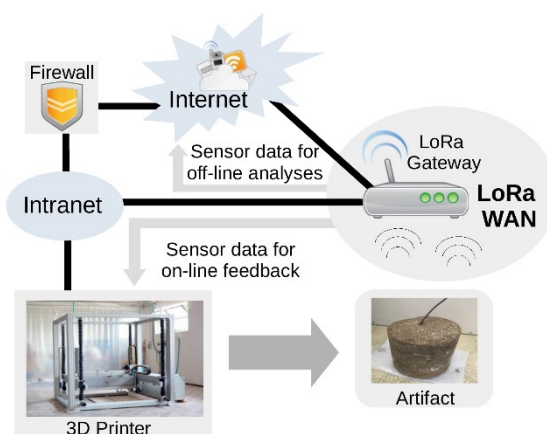


Figure 1. Automation System of the 3D Printer

Table 1. Transmission periods and data payloads.

Phase	Period	Data Amount per Sensor
Production	≤ 300 s	20 bytes
Final Deployment	≥ 3600 s	20 bytes

sensors that act as LoRaWAN End Devices (EDs). After production, the final deployment phase begins, the artifacts are placed in their final locations and the LoRaWAN Gateway device is positioned within range of the sensors and connected to the Internet. This allows sensor data to be transmitted to a remote cloud for offline analysis.

For the sake of clarity, the two types of sensor data transmission shown in Figure 1 (referred to as “sensor data for on-line feedback” and “sensor data for off-line analysis”, respectively) will never occur simultaneously. In fact, during the production phase of an artifact, only the Intranet connection is used, while during the final deployment phase, only the Internet communication is active.

Battery lifetime of embedded sensors is strongly influenced by the periodicity of their transmission as well as the amount of data transmitted, which directly affects the time required for each transmission. In fact, transmission is the operating situation where the LoRa interface of the sensors has the higher power consumption. In the context of the intended application, the transmission time depends on the operational phase (production or final deployment), while the amount of data transmitted remains the same throughout the life of the artifacts. Obviously, during the production of an artifact, short transmission times are required (relative to the time needed to produce the artifact), since sensor data is used for on-line feedback. Conversely, in the final deployment phase, there is no need for strict timing and periods can be relaxed. Table 1 shows the typical values of periods and amount of data exchanged used in the following battery life analysis.

3. RELATED WORKS AND CONTRIBUTION

Some interesting contributions dealing with the power consumption aspects of LPWANs are available in the scientific literature. In [17], the authors provide a comprehensive assessment of the power consumption of commercially available modules by defining theoretical models based on real data obtained from experimental sessions. In [18], the energy consumption of a solid waste management system is addressed in a simulated scenario that also allows the estimation of battery life. Similarly, the authors of [19] present a self-optimizing wireless water level monitoring system that can improve battery life based on operating conditions. Energy consumption is also a major constraint for the authors of [20], where a LoRa-based localization system is addressed. In [21], a battery lifetime analysis is proposed. Interestingly, it refers to LoRa sensors deployed in manholes, which are difficult to access for maintenance purposes.

Nevertheless, an effective a priori estimation of the battery lifetime is crucial in the AM application targeted in this manuscript, and this can only be achieved with accurate battery discharge models. In this direction, models based on machine learning (ML) techniques have already been successfully applied, since they allow to easily take into account the non-linearities that often occur in this context. For example, in [22], an ML-based system was used to detect the end of battery life. Furthermore, in [23]-[27], ML techniques are used to build models for the state

of charge, discharge curves, and lifetime prediction of lithium batteries. Unfortunately, the models proposed in these works cannot be considered in ADMIN-4D because the artifacts produced would be expected to operate even under potentially extreme weather conditions. Actually, these models were developed for generic lithium batteries, but for the intended application, heavy lithium batteries were chosen that present very different characteristics.

This highlights the importance of defining a more comprehensive battery discharge model, capable of capturing the effect of battery performance under different usage conditions, such as temperature variations or different configurations of sensor communication parameters. Such a model would be an essential tool for the design of systems using battery-powered sensors, as it would allow the lifetime of the sensors to be estimated based on the conditions in which they will be used, and therefore decide which communication parameters and sensor suite to use to ensure maximum battery life. It is important to note that battery discharge curves are generally obtained using static parameters such as temperature and discharge current. In reality, however, sensors often operate under dynamic conditions where these parameters can vary continuously. Therefore, it is necessary to use battery discharge models that take these variables into account to obtain more accurate results. Moreover, given the multiple nonlinearities of the batteries under consideration, the ability to simulate the discharge process dynamically and under different conditions allows to predict in advance possible problems in the on-board sensors, such as those due to voltage and temperature variations, allowing improvements and optimizations of the measurement system before the final deployment.

4. SENSORS AND BATTERIES SELECTION

In consideration of the peculiarities of the AM application described in the previous sections, the board hosting sensors and communication interfaces, which must be embedded within the manufactured artifact, should also present suitable mechanical and waterproof properties. We identified a good candidate in the Tinovi PM-IO-5-SM device [28], which can host different type of sensors and is already equipped with a LoRa interface, hence acting as a LoRaWAN end device in the targeted LoRaWAN sensor network scenario. In the adopted configuration, the Tinovi system provide both humidity and temperature measurements (the latter in the range [-20, 70] °C with an uncertainty of 0.6 °C) transmits information about the battery state of charge with a good resolution. Another important consideration is that the LoRa interface of such sensors can be configured using Over-The-Air Activation (OTAA) mode to activate the end device. In fact, artifacts are typically moved from the production site to the final deployment site, so the sensors need to be able to join different LoRaWAN networks during their lifetime. Considering that the sensor becomes inaccessible after production, the sensor must use OTAA so that the device address and session key required to join a network are dynamically assigned. OTAA also allows network parameters (e.g., measurement’s transmission period) to be changed remotely and dynamically.

The Tinovi sensors can be powered by different types of batteries. We have considered those listed in Table 2, where they are compared for energy density and temperature range. In fact, the specific AM printing process requires the batteries to work in a wide temperature range. For this reason, we chose lithium

Table 2. Comparison of different battery chemistries.

Chemistry	Energy density (W h L ⁻¹)	Temperature range (°C)
Sealed Lead Acid (SLA)	70	-40 / +60
Alkaline (Zn – MnO ₂)	340	-20 / +70
Lithium cobalt oxide (LiCoO ₂)	560	-20 / +60
Lithium manganese nickel (LiNiMnCoO ₂)	580	-20 / +60
Lithium thionyl chloride (LiSOCl ₂)	350	-60 / +85

thionyl chloride (LiSOCl₂) batteries. In fact, they are specifically designed to operate over a wide [-60, +85] °C temperature range, which makes them suitable for military and medical applications, locking mechanism or metering applications that require long life without the need to replace the battery [29]–[30]. It should be noted that ADMIN-4D also requires a sufficient energy density to keep the size of the batteries as small as possible and to ensure that they can be easily inserted into the artifacts. For this reason, the widespread and cheap SLA batteries are not considered in this study. Furthermore, the energy density of the selected LiSOCl₂ batteries is considered sufficient for the application.

4.1. Modelling of Lithium Thionyl Chloride batteries

In a first stage, SAFT LS 17500 LiSOCl₂ batteries were tested as they are widely available off-the-shelf [31]. Their main characteristics are summarized in Table 3.

Unfortunately, the battery manufacturer does not provide a public dataset for the different measurements provided in the battery datasheet. For this reason, we have derived our data from the graphs contained in the datasheet using a graphical data extraction method. The available data consists of i) voltage profiles, ii) the correlation between plateau voltage and current drawn at different temperatures and, finally, iii) the relationship between capacity and current drawn at different temperatures. The results of this extraction are represented with solid lines in Figure 2, Figure 3, and Figure 4. Considering the high resolution of the available images, the accuracy with which the curves are reproduced here is rather good. Indeed, it is also possible to provide an estimate of the uncertainty associated to the data points. In fact, each curve has been originally sampled with 25 data points, and for Figure 2 we have a maximum uncertainty of 2.3 mV, while for Figure 3 it is 4.5 mV. For the data points related to capacity in Figure 4 the uncertainty is 23 mA h.

As can be seen in Figure 2, the discharging profiles strongly depend on the current drawn, i.e., the current absorbed by the battery. The longest lifetime is 2523 hours, obtained with constant 1.3 mA current. It can also be seen that the level of the plateau voltage decreases gradually at higher current levels. This effect is due to the high nonlinear internal resistance, estimated to be 13.6 Ω on average. This voltage drop is not a negligible effect, as the drop below the minimum operating voltage of the sensor can affect its actual functionality.

Table 3. SAFT LS 17500 battery specification.

Description	Specification
Rechargeable	No
Nominal Voltage	3.60 V
Nominal Capacity	3600 mA h
Nominal cut-off voltage	3.3 V
Operating Temperature	-60 °C to 85 °C

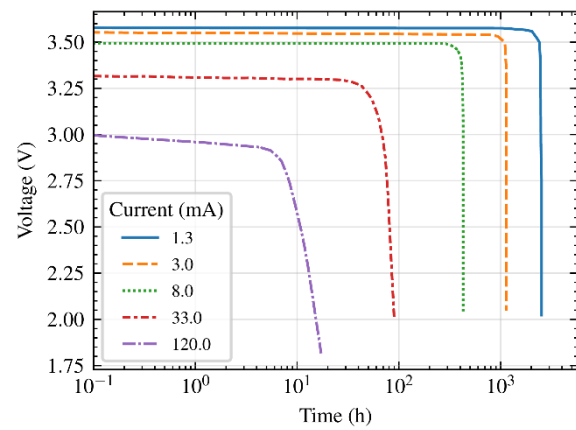


Figure 2. Typical discharge profile at 20 °C for the SAFT LS 17500 battery. Extracted from [26].

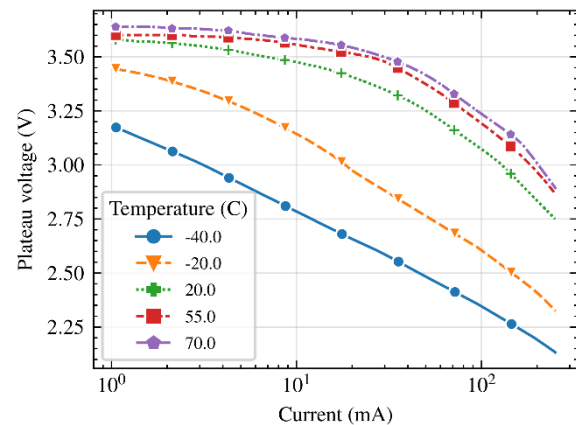


Figure 3. Dependence of the plateau voltage from current drawn at different temperatures. Extracted from [26].

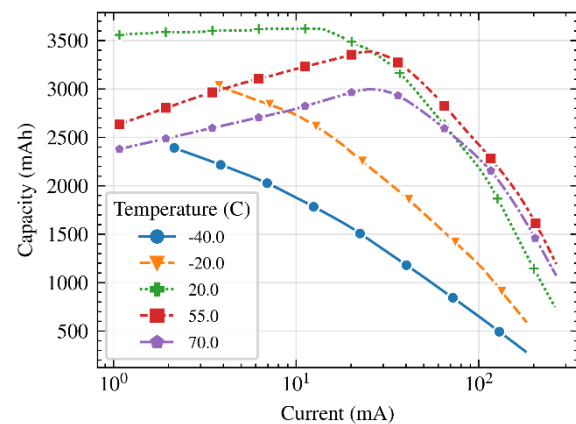


Figure 4. Dependence of the total available capacity from current drawn at different temperatures. Extracted from [26].

The voltage variations are also evident considering discharge curves at different temperatures, as reported in Figure 3. As can be seen, for a given current, there are considerably different plateau voltage values, depending on the working temperature. This behaviour may represent an issue in several applications (the ADMIN-4D project is one of them, actually) where the batteries used to feed the sensors are exposed to highly variable climatic conditions.

Temperature and current drawn also impact on the total available battery capacity. From Figure 4, it is clear that these

types of cells are susceptible to the Peukert's effect [32], which lowers down the total available battery capacity depending on the current draw and temperature, with the consequent reduction of the battery lifetime.

It can be concluded that the design of an accurate battery lifetime model is a challenging task that requires the consideration of several different aspects. Admittedly, accurate models can be developed by exploiting the equations describing the chemical interaction between the anode and cathode. Such models allow to obtain a very high accuracy, since they depend on the intrinsic parameters of the battery. Unfortunately, they are difficult to define and tune for commercially available cells, since the information available for such devices is typically insufficient.

Therefore, to address this challenge, in this work we have adopted a hybrid approach, where a suitably tuned generic battery dynamic model is used in conjunction with a data-driven approach based on Artificial Neural Networks. In the following section, we will discuss the tuning of the first dynamic model, while the ANN approach will be discussed in Section 7.

5. TUNING OF THE GENERIC BATTERY DYNAMIC MODEL

Several models for generic purpose lithium-ion based batteries have been proposed in the scientific literature. A widely used one is discussed in [33] and its implementation is currently found in Matlab Simscape under the name Generic Battery Dynamic Model, hereafter referred to as GDBM. This model actually describes the behaviour of a generic rechargeable battery using a combination of three stages. First, a (short) exponential voltage drop occurs suddenly when the battery is fully charged and starts to deliver energy; this is followed by a so-called nominal region (a plateau region) where the energy is delivered from the battery with a quasi-constant voltage level until the voltage starts to drop below the nominal battery voltage level. The third section is related to the sudden loss of energy, where the battery is discharged, and the voltage drops abruptly. The GDBM is implemented by an equivalent feedback system, whose parameters can be tuned to adequately model different battery typologies and their discharge characteristics.

In this regard, we considered the parameters provided by the battery manufacturer, in particular the discharge profiles specific to the SAFT LS 17500 $LiSOCl_2$ batteries shown in the previous Figure 2 to Figure 4. From the discharge profile at the nominal current of 1.3 mA, we were able to extract the required model parameters that are reported in Table 4. The tuning process of the GDBM model resulted in the discharge curves shown in Figure 5, that have been subsequently derived for different current values (solid lines) and compared with those reported in the battery datasheet (dotted lines).

Table 4. Parameters of the GDBM model, for the characterization of the discharge profile.

Parameter	Value
Nominal voltage	3.6 V
Maximum capacity	3.6 A h
Fully charged voltage	3.67 V
Nominal discharge current	1.3 mA
Internal resistance	13.6 Ω
Nominal ambient temperature	20 °C
Second ambient temperature	-40 °C
Maximum capacity at -40 °C	2.744 A h
Initial discharge voltage at -40 °C	3.12 V

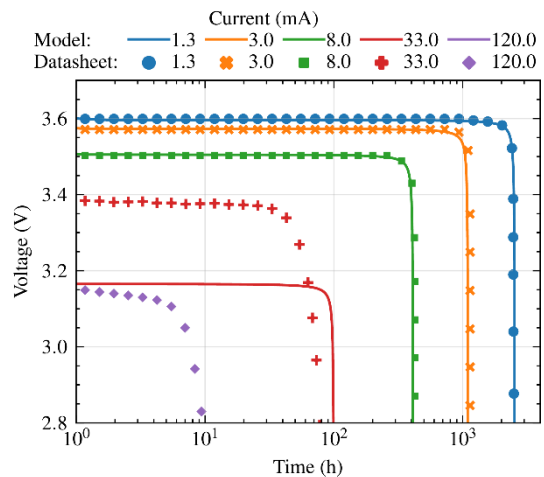


Figure 5. Comparison between the discharge profiles at 20 °C extracted from the datasheet (dotted lines) and derived from the tuned GDBM model (solid lines), for 5 different current values.

As can be observed in the figure, the model discharge profiles (and thus the lifetime estimate) are in good agreement with those declared by the manufacturer for current values of 1.3, 3 and 8 mA. For higher currents, the experimental and model trends are completely different to the point that the model estimate of the discharge profile at 120 mA is completely inconsistent with the experimental one (in fact, it is not even visible in the plot).

The above voltage profiles can be compared from a numerical point of view by looking at both the average deviation between the experimental and model curves and the predicted battery life. The former can be evaluated by the Root Mean Square Error (RMSE), calculated as the root of the average squared deviations between the model predicted value and the expected voltage level of the battery, as extracted from the manufacturer's discharge curve for a given current and after a given time. Table 5 reports the obtained values, where it can be observed that the RMSE is relatively low for low currents and consistently increases as the current increases. Analogously, the same trend can be observed in the lifetime estimation, although in a less obvious way, because the estimated lifetime is only consistent with the nominal current of 1.3 mA used for the tuning process.

The obtained results are not surprising since, as already pointed out, the lithium chloride thionyl batteries present a considerable internal resistance that varies non-linearly with the current draw. Also, such batteries are affected by the Peukert's effect, and the resistance is almost constant at the nominal current and tends to decrease at higher currents. Unfortunately, this model does not consider these effects since, as a matter of fact, it keeps the resistance constant for every current draw, so that the Peukert's effect is not considered at all.

Table 5. Comparison between the discharge profile (at 20 °C) extracted from the datasheet and the GDBM model.

Current (mA)	Lifetime (h)			RMSE in voltage profile (V)
	Datasheet	Estimated	Error (%)	
1.3	2523.88	2523.92	0.00	$2.97 \cdot 10^{-4}$
3.0	1140.39	1093.70	4.09	$1.03 \cdot 10^{-3}$
8.0	425.76	410.14	3.67	$1.47 \cdot 10^{-3}$
33.0	90.38	99.43	10.02	$1.18 \cdot 10^{-1}$
120.0	17.20	27.34	58.95	$9.73 \cdot 10^{-1}$

As discussed earlier, temperature is another source of complexity and nonlinearity that the GDBM takes into account, although it cannot reproduce the same behaviour as the lithium chloride thionyl batteries. This is visually illustrated in Figure 6, which shows the discharge profile obtained at a constant discharge current of 1.3 mA for different temperatures. In the figure, five different temperatures are considered, and the discharge curves obtained from the GDBM are shown with solid lines, while the manufacturer's curves are shown with dotted lines. The graph clearly indicates that the match between model and datasheet is rather satisfactory only for temperatures of 20 °C and -40 °C, that are those used for tuning the model, as reported in Table 4. Conversely, for other temperatures a significant discrepancy can be observed, for example, at 55 °C and 70 °C. Looking at Figure 6, it can also be observed that both the plateau voltage and total capacity depend on the temperature in a strongly non-linear way. Moreover, in the leftmost part of the solid GDBM curves, the exponential variation of the voltage is evident (notice that it is linear since the x-axis is in logarithmic scale). This behaviour is less evident only for $T = 20\text{ }^{\circ}\text{C}$ in both Figure 5 and Figure 6, since the model is tuned around that temperature, confirming the temperature dependence.

The results obtained from the tuned GDBM model suggest that it is able to provide a satisfactory description of the main features of the discharge behaviour for the adopted LiSOCl_2 batteries but limited to the cases close to the operating points selected for the model calibration. In the next section, a proposal to overcome this limitation is presented, based on a data-driven approach to be used in conjunction with the GDBM approach.

6. A DATA-DRIVEN DISCHARGE MODEL

Models based on a data-driven approach may prove advantageous to address the negative effects due to non-linearities that are experienced with models based on battery parameters, such as the GDBM discussed in the previous section [34]. In particular, an approach that has already proven its effectiveness [35] relies on the use of Artificial Neural Networks (ANNs) to profitably approximate the nonlinear functions related to the battery discharge behaviour with the desired accuracy. Therefore, to address the issues of the dynamic battery model that have been highlighted in the previous section, in

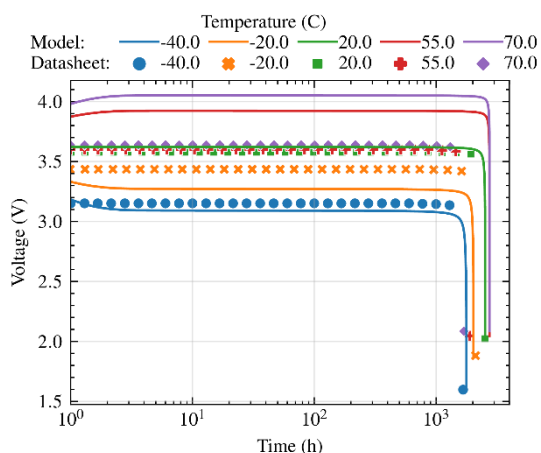


Figure 6. Comparison between the discharge profile extracted from the datasheet (dotted lines) and the GDBM model (solid lines) at different temperatures. All the curves are obtained considering a constant discharge current of 1.3 mA.

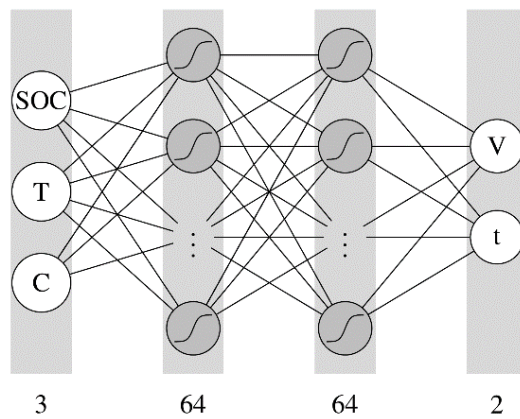


Figure 7. Structure of the adopted MLPNN.

particular related to the nonlinear dependence with the temperature and the internal resistance, we exploited a suitable ANN with the aim of increase the estimation accuracy of the lifetime duration of LiSOCl_2 batteries.

In particular, we implemented a Multiple-Layer Perceptron Neural Network (MLPNN) since it demonstrated to be promising in solving similar problems [36]. The structure of the MLPNN is shown in Figure 7. In the input layer, the input parameters are State of Charge (SOC), temperature (T) and current drawn (C). Two hidden layers, each with 64 neurons, realize the non-linear transformation from the input layer. Finally, the output layer provides battery voltage (V) and lifetime estimation (t).

The structure of the MLPNN was chosen with an embedded system implementation in mind, so that it can be deployed directly in the sensor, which can change the period and transmission parameters based on the estimated duration. In particular, the minimum number of neurons and hidden layers was chosen to solve the estimation problem without causing overfitting problems, while ensuring low memory consumption and computation time.

The training and validation phases of the applied ANN clearly require a consistent and sufficiently large dataset. Unfortunately, as mentioned in Section 4.1, the battery manufacturer does not provide a public dataset for the different measurements provided in the battery datasheet, which led us to use a graphical extraction procedure. In order to obtain an adequate amount of data to train and then identify complex relationships between inputs and outputs, we needed to apply a data augmentation technique to artificially increase the size of the dataset from the initial 25 points. To do this, we used a spline curve to fit the original raw data points while minimizing the RMSE. Given the low uncertainty associated with the extracted data, and the fact that the RMSE in this fit was kept extremely low, the uncertainty associated with the data inferred from the spline can be considered consistent with those revealed in Section 4.1.

The obtained augmented dataset consists of 250000 unique entries, which were split between training and validation in a ratio of 80%-20%. Other meaningful hyperparameters are shown in Table 6.

As shown in Table 6, the number of training epochs was set to 150. This value was determined using the early stopping technique to avoid overfitting. The trends of training and validation loss are shown in Figure 8. As can be seen from the figure, both training and validation loss decrease with the number of epochs and almost reach zero. After training the

Table 6. Parameters for the characterization of the discharge profile in the MLPNN model.

Parameter	Value
Activation function	Tanh
Loss function	MSE
Optimizer	Adam
Learning rate	0.0001 (non-scheduled)
Epoch	150
Batch size	512

Table 7. Comparison between the discharge profile at 20 °C extracted from the validation dataset and the MLPNN model.

Current (mA)	Lifetime (h)			RMSE in voltage profile (V)
	Datasheet	Estimated	Error (%)	
1.3	2523.88	2568.19	1.76	$3.10 \cdot 10^{-4}$
3.0	1140.39	1122.50	1.56	$7.41 \cdot 10^{-5}$
8.0	425.76	425.52	0.06	$9.33 \cdot 10^{-5}$
33.0	90.38	89.21	1.29	$2.57 \cdot 10^{-5}$
120.0	17.20	16.94	1.51	$1.19 \cdot 10^{-5}$

model, its behaviour was compared with the experimental data obtained from the manufacturer. The results of modelling with the MLPNN are shown in Figure 9, where the discharge profiles obtained for different currents are reported. Table 7 provides more detailed statistics.

As can be seen, the results obtained are better than those obtained with the GBDM model. In fact, although the percentage error of the lifetime estimation at 1.3 mA is higher than that of the GBDM model, the lifetime estimation error is limited to 2% over the whole discharge current range. The accuracy of the model on the test data set is also confirmed by the RMSE in the voltage profile, which is definitely very limited. While for the GBDM model both the lifetime estimation error and the MSE increase moving away from the profile where the tuning was performed, the MLPNN keeps both metrics bounded and rather stable over the different profiles. The advantage of using such a model seems clear. In fact, it is able to better generalize the estimation problem, giving a higher accuracy in a wide range of operating conditions.

These considerations can be further confirmed by the discharge profiles obtained for a constant current of 1.3 mA, but for different temperatures. This comparison is shown in Figure 10, whereas some statistical details are reported in Table 8. Even in this case, the discharge profiles as well as the lifetime estimations agree with the experimental ones with a very good accuracy, and an estimation error under 6% in the worst case.

7. EXPERIMENTAL ASSESSMENT OF THE PROPOSED DISCHARGE MODELS

In order to evaluate the effectiveness of the proposed models, we first performed some experimental tests on the Tinovi smart sensor alone. The goal is to verify whether the proposed models, tuned on the data provided by the manufacturer, are able to provide a consistent prediction of the actual battery behaviour in the final system. To increase the reproducibility of the experiments, the experimental sessions were conducted in a room with a controlled temperature of 20°C, with the Tinovi device (namely, the LoRaWAN ED) placed 1 m away from the LoRaWAN gateway.

Table 8. Comparison between the discharge profile at constant discharge current 1.3 mA for different temperatures.

Temperature (°C)	Lifetime (h)			RMSE in voltage profile (V)
	Datasheet	Estimated	Error (%)	
-40.0	1666.21	1760.29	5.65	$3.17 \cdot 10^{-4}$
-20.0	2110.56	2233.70	5.83	$3.44 \cdot 10^{-4}$
20.0	2523.66	2568.19	1.76	$3.10 \cdot 10^{-4}$
55.0	1883.47	1944.04	3.22	$3.33 \cdot 10^{-4}$
70.0	1688.57	1711.55	1.36	$3.31 \cdot 10^{-4}$

The adopted Tinovi PM-IO-5-SM smart sensor is configured to transmit in each LoRaWAN frame an internal reading of the battery voltage, whose value is encoded in binary format to map the range from 2.8 V to the maximum value of 4.2 V reached during charging. The resolution of the voltage reading is 1%, which correspond to 14 mV. During these tests, the sensor is configured to transmit a packet with a period of five (5) minutes, containing the measured variables (mostly, temperature and humidity) and the information about the battery status. It should be noted that the sensor can be in two different states, active and sleep: the former is the state in which the sensor is either sending or receiving data from its probes, while the latter is the idle state in which the sensor does not perform any action. The main

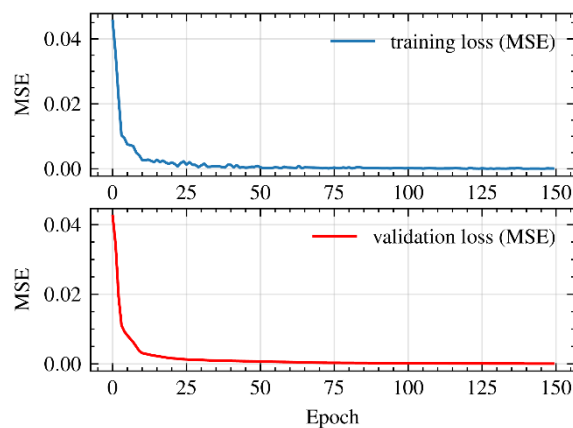


Figure 8. Training and validation loss.

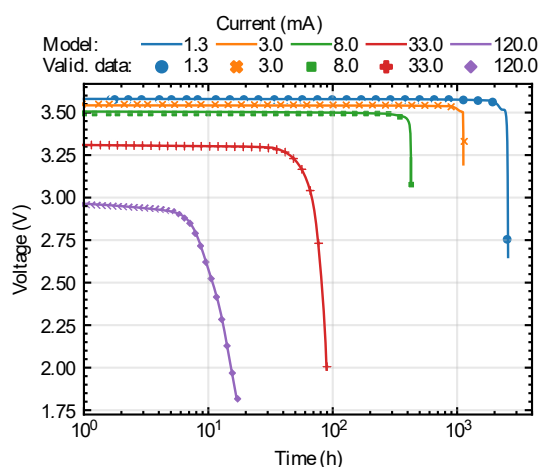


Figure 9. Comparison between the discharge profile at 20 °C on the test dataset and the one generated by the MLPNN. Markers represent the test data while solid lines represent the data generated by the model.

Table 9. Parameters adopted in the experimental setup.

Parameter	Value
Transmission frequency	868 MHz
Spreading factor	7
Bandwidth	125 kHz
Code rate	4/5
Payload length	20
Sleep time	300 s
Wake-up + acquisition + transmission time	~ 5 s
Sleep current consumption	0.15 mA
Active current consumption	150 mA
Average current consumption	2.6 mA
Module operating temperature range	-20 °C – +70 °C
Voltage operating range	2.5 V – 6 V
Output power	14 dBm

parameters used to configure the Tinovi smart sensor during these experimental sessions are shown in Table 9.

The average current consumption of the sensor, as shown in the table, is 2.6 mA. We have therefore used the two proposed models to generate the corresponding discharge curves for this specific current and at a constant temperature of 20°C. The estimates of the voltage profiles were then compared with the results of the real voltage measurements taken by the sensor. The results are shown in Figure 11 and Table 10, respectively.

The comparison highlights that both models produce similar discharge profiles, and in a rather good accordance with each other. In particular, the MLPNN is able to better approximate the nominal (plateau) voltage phase and is very close to the actual measured final fast discharge phase. Conversely, the GBDM is more precise at modelling the starting point and the initial part of the discharge phase, where the voltage starts to drop below the nominal value. Definitely, MLPNN provides a higher accuracy in the prediction of both the voltage values and the total battery lifetime, as can be seen from Table 10. In fact, the GBDM model tends to overestimate the plateau and to slightly underestimate the lifetime of the battery.

Another aspect that affects the power consumption of the sensor is the spreading factor (SF) adopted by the LoRa modules.

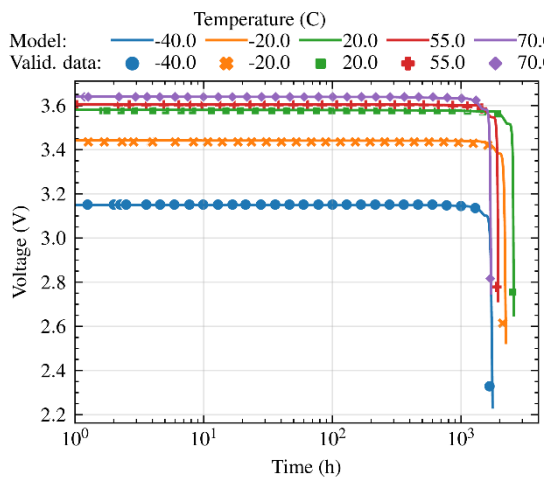


Figure 10. Comparison between the discharge profiles from the validation dataset and the ones generated by the MLPNN, at different temperatures. Markers represent the validation data while line represent the data generated by the model. All the curves are obtained considering a constant discharge current of 1.3 mA.

Table 10. Evaluation statistics relevant to the curves in Figure 11.

	Lifetime (h)	Lifetime error (%)	RMSE (V)
Experimental	1323.94	-	-
MLPNN	1322.32	0.12	$2.33 \cdot 10^{-4}$
GBDM	1302.38	1.63	$1.06 \cdot 10^{-3}$

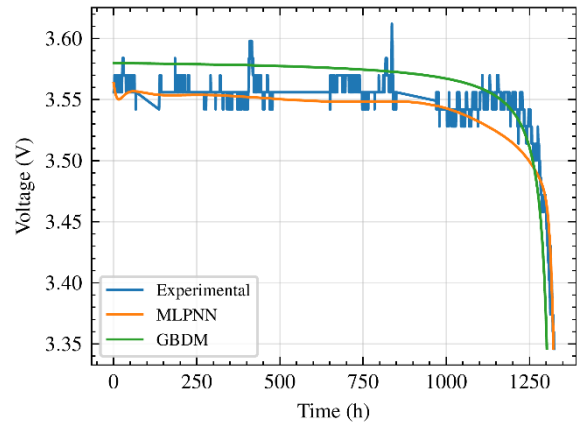


Figure 11. Comparison between the discharge profiles generated by the MLPNN and the GBDM models, with respect to the experimentally measured one. Controlled environment, T = 20 °C, sensor only.

In fact, the use of a higher SF (at the same transmit power, of course) allows a more robust transmission, but at the cost of longer transmission times, which consequently result in a higher power consumption of the whole sensor. For example, in the case of the Tinovi PM-IO-5-SM, the transmission of 20 Bytes with SF12 increases the time in the active state of the ED from 5 s to 6 s (remember that the packet airtime with SF12 is 1810 ms). As a result, the average current required increases from 2.6 mA to 3.1 mA, with a corresponding decrease in battery life.

Based on the outcomes of the previous experiment, the MLPNN model can be profitably exploited to estimate the battery lifetime both at different temperatures and for a higher SF. The results of this analysis are shown in Table 11, which confirms a decrease of about 16-17% in battery life when moving from SF = 7 to SF = 12.

8. BATTERY LIFE ESTIMATION IN THE ADMIN-4D APPLICATION CONTEXT

In this section, the developed battery models have been used to estimate the lifetime in the real application context, i.e., considering the whole 3D printing process of an artifact (production phase) and its subsequent positioning at the final site (deployment phase), where sensor data is transmitted to the remote cloud. It should be noted that the production of a real

Table 11. Battery lifetime estimation using the MLPNN model at different temperatures for SF = 7 and SF = 12.

	Temperature (°C)	Lifetime (h)
SF = 7	-20	1126.90
	20	1323.94
	70	938.56
SF = 12	-20	928.30
	20	1112.94
	70	784.43

artifact is a process that takes 72 h. In this phase, the sleep time of the LoRaWAN EDs (which corresponds to the period of sensor data transmission) was set to 300 s, in accordance with the values given in Table 1. Subsequently, in the final deployment phase, the sleep time was increased to 3600 s in order to maximize battery life while maintaining the required periodicity of measurement data for monitoring purposes. With these values for the sleep period duration, the resulting average current consumption is about 2.6 mA in the production phase and 0.35 mA in the final deployment phase.

The two phases are clearly very different from each other, both in terms of power consumption and temperature range. Moreover, the production phase is characterized by strong temperature variations, as experimentally observed, which range from 20 °C to 70 °C. From the analysis carried out in the previous sections, none of the models considered is able to satisfactorily emulate both phases. Indeed, in the production phase, the GBDM model appears unsuitable due to the high temperature dynamics, while the MLPNN shows a good behaviour with respect to this type of operating conditions. Conversely, in the deployment phase, which is practically static, the GBDM is more effective, taking into account the fact that the MLPNN provides inconsistent estimates, since this model has not been trained for the low current that characterizes such a phase. As a consequence, we adopted a hybrid approach to model the discharge curve in a real application context. Specifically, the MLPNN model is used for the production phase and the GBDM for the deployment one.

Figure 12 shows the resulting voltage profile obtained with this hybrid approach. As can be seen, there is a slight voltage increase in the initial part (see the inner rectangle showing the curve from 0 to 100 hours) due to the increase in temperature. This is followed by the expected voltage plateau and finally by the rapid voltage drop. Note that the glitch at $t = 72$ hours is due to the switch between the two models. It represents the initial rapid exponential part of the discharge curve typical of the GBDM model.

Taking into account the assessment of the tuned models made in the previous sections, the results obtained in this last analysis allowed to estimate the battery lifetime, for the final application conditions, to be up to 9104 hours. This corresponds to more than one year during which the sensor is able to send useful monitoring data. In fact, this value meets the requirements of the ADMIN-4D project.

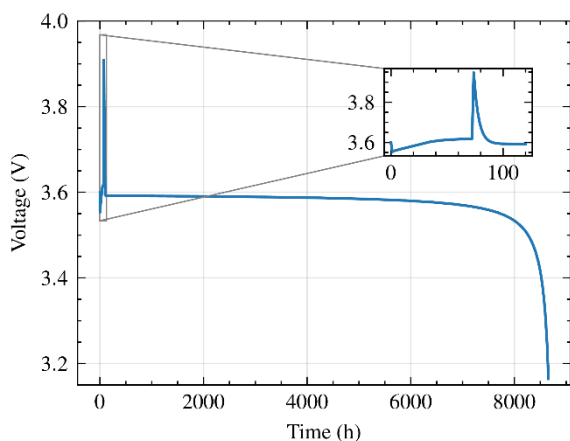


Figure 12. Voltage profile during the production and deployment phases.

9. CONCLUSIONS AND FUTURE DIRECTIONS OF RESEARCH

This paper presents an additive manufacturing experiment in which battery-powered sensors are embedded in the manufactured artifacts. Since the sensors are inaccessible after manufacturing, the acquisition of their measurements is totally conditioned by the lifetime of the batteries.

Therefore, we investigated the possibility of modelling the discharge curve of the batteries in order to estimate their lifetime, taking into account the challenging operating conditions imposed by the targeted application. For this purpose, an innovative model based on an Artificial Neural Network (ANN), specifically a MLPNN, has been proposed and developed starting from the discharge curve of the adopted lithium-thionyl chloride batteries. The model has been used in conjunction with a popular one, namely the GBDM, realizing a hybrid approach that proved effective for the battery lifetime estimation. Both models have been calibrated using information from the battery datasheet and validated using measurements obtained from actual sensors.

The ADMIN-4D project has been completed and some prototype artifacts have already been produced and positioned at the partners' sites where they transmit sensor data as described for the final deployment phase. This scenario paves the way for some interesting future activities. The first, related to the follow-up of the project, is represented by the off-line analyses that will provide data to better tune the upcoming artifact production. Second, and more focused on the topics of this paper, the MLPNN model needs to be further refined to become effective also for low currents. In this respect, the data coming from the currently installed artifacts will prove particularly useful, since they can be used to perform a more extensive and precise training and validation process of the model.

REFERENCES

- [1] S. Serroni, M. Arnesano, L. Violini, G. M. Revel, An IoT measurement solution for continuous Indoor environmental quality monitoring for buildings renovation, *Acta IMEKO* 10 (2021) 4, art. 35, pp. 230 - 238. DOI: [10.21014/acta_imeko.v10i4.1182](https://doi.org/10.21014/acta_imeko.v10i4.1182)
- [2] V. Alcácer, V. Cruz-Machado, Scanning the Industry 4.0: A Literature Review on Technologies for Manufacturing Systems, *Engineering Science and Technology, an International Journal*, vol. 22, no. 3, 2019, pp. 899–919. DOI: [10.1016/j.jestch.2019.01.006](https://doi.org/10.1016/j.jestch.2019.01.006)
- [3] E. Oztemel, S. Gursev, Literature review of Industry 4.0 and related technologies, *Journal of Intelligent manufacturing*, vol. 31, 2020, pp. 127–182. DOI: [10.1007/s10845-018-1433-8](https://doi.org/10.1007/s10845-018-1433-8)
- [4] E. Balestrieri, L. De Vito, F. Lamonaca, F. Picariello, S. Rapuano, I. Tudosa, Research challenges in measurements for Internet of Things systems, *Acta IMEKO* 7 (2018) 4, art. 14, pp. 82-94. DOI: [10.21014/acta_imeko.v7i4.675](https://doi.org/10.21014/acta_imeko.v7i4.675)
- [5] L. Fratocchi, C. Di Stefano, Industry 4.0 technologies and manufacturing back-shoring: A European perspective, *Acta IMEKO* 9 (2020) 4, pp. 13 - 20. DOI: [10.21014/acta_imeko.v9i4.721](https://doi.org/10.21014/acta_imeko.v9i4.721)
- [6] G. Allevi, L. Capponi, P. Castellini, P. Chiariotti, F. Docchio, F. Freni, R. Marsili, M. Martarelli, R. Montanini, S. Pasinetti, A. Quattrocchi, R. Rossetti, G. Rossi, G. Sansoni, E. P. Tomasini, Investigating additive manufactured lattice structures: A multi-instrument approach, *IEEE Transactions on Instrumentation and Measurement*, vol. 69, no. 5, 2020, pp. 2459–2467. DOI: [10.1109/TIM.2019.2959293](https://doi.org/10.1109/TIM.2019.2959293)
- [7] M. Grasso, A. Remani, A. Dickens, B. M. Colosimo, R. K. Leach, In-situ measurement and monitoring methods for metal powder

- bed fusion: An updated review, *Measurement Science and Technology*, vol. 32, no. 11, p. 112001, Jul. 2021.
DOI: [10.1088/1361-6501/ac0b6b](https://doi.org/10.1088/1361-6501/ac0b6b).
- [8] T. Fedullo, A. Morato, G. Peserico, L. Trevisan, F. Tramarin, S. Vitturi, L. Rovati, An IoT Measurement System Based on LoRaWAN for Additive Manufacturing, *Sensors*, vol. 22, no. 15, 2022. Online [Accessed 21 March 2023]
<https://www.mdpi.com/1424-8220/22/15/5466>
 - [9] M. Grasso, B. M. Colosimo, Process defects and in situ monitoring methods in metal powder bed fusion: A review, *Measurement Science and Technology*, vol. 28, no. 4, Feb. 2017, p. 044005.
DOI: [10.1088/1361-6501/aa5c4f](https://doi.org/10.1088/1361-6501/aa5c4f).
 - [10] S. Vitturi, L. Trevisan, A. Morato, G. Frigo, F. Tramarin, Evaluation of LoRaWAN for Sensor Data Collection in an IIoT-based Additive Manufacturing Project, 2020 IEEE Int. Instrumentation and Measurement Technology Conf. (I2MTC), Dubrovnik, Croatia, 25-28 May 2020, pp. 1–6.
DOI: [10.1109/I2MTC43012.2020.9128684](https://doi.org/10.1109/I2MTC43012.2020.9128684)
 - [11] S. Spinsante, L. Gioacchini, L. Scalise, A field-measurements-based LoRa network planning tool, *Acta IMEKO 9 (2020) 4*, pp. 21–29.
DOI: [10.21014/acta_imeko.v9i4.725](https://doi.org/10.21014/acta_imeko.v9i4.725)
 - [12] M. Luvisotto, F. Tramarin, L. Vangelista, S. Vitturi, On the Use of LoRaWAN for Indoor Industrial IoT Applications, *Wireless Communications and Mobile Computing*, vol. 2018, p. 11.
DOI: [10.1155/2018/3982646](https://doi.org/10.1155/2018/3982646)
 - [13] T. Fedullo, A. Morato, F. Tramarin, P. Bellagente, P. Ferrari, E. Sisinni, Adaptive LoRaWAN transmission exploiting reinforcement learning: The industrial case, 2021 IEEE Int. Workshop on Metrology for Industry 4.0 and IoT, MetroInd 4.0 and IoT 2021, Rome, Italy, 7-9 June 2021, pp. 671–676.
DOI: [10.1109/MetroInd4.0IoT51437.2021.9488498](https://doi.org/10.1109/MetroInd4.0IoT51437.2021.9488498)
 - [14] L. Trevisan, S. Vitturi, F. Tramarin, A. Morato, An IIoT System to Monitor 3D-Printed Artifacts via LoRaWAN Embedded Sensors, IEEE Int. Conference on Emerging Technologies and Factory Automation (ETFA), Vienna, Austria, 8-11 September 2020, pp. 1–4.
DOI: [10.1109/ETFA46521.2020.9212019](https://doi.org/10.1109/ETFA46521.2020.9212019)
 - [15] F. Zonzini, C. Aguzzi, L. Gigli, L. Sciuillo, N. Testoni, L. De Marchi, T. S. Cinotti, C. Mennuti, A. Marzani, Structural Health Monitoring and Prognostic of Industrial Plants and Civil Structures: A Sensor to Cloud Architecture, *IEEE Instr. & Measurement Magazine*, vol. 23, no. 9, 2020, pp. 21–27.
DOI: [10.1109/MIM.2020.9289069](https://doi.org/10.1109/MIM.2020.9289069)
 - [16] G. Di Renzone, E. Landi, M. Mugnaini, L. Parri, G. Peruzzi, and A. Pozzebon, Assessment of LoRaWAN transmission systems under temperature and humidity, gas, and vibration aging effects within IIoT contexts, *IEEE Transactions on Instrumentation and Measurement*, vol. 71, 2022, pp. 1–11.
DOI: [10.1109/TIM.2021.3137568](https://doi.org/10.1109/TIM.2021.3137568)
 - [17] S. Ould, N. S. Bennett, Energy performance analysis and modelling of LoRa prototyping boards, *Sensors*, vol. 21, no. 23, 2021, 17 pp.
DOI: [10.3390/s21237992](https://doi.org/10.3390/s21237992)
 - [18] S. V. Akram, R. Singh, M. A. AlZain, A. Gehlot, M. Rashid, O. S. Faragallah, W. El-Shafai, D. Prashar, Performance analysis of IOT and long-range radio-based sensor node and gateway architecture for solid waste management, *Sensors*, vol. 21, no. 8, 2021.
DOI: [10.3390/s21082774](https://doi.org/10.3390/s21082774)
 - [19] T.-K. Chi, H.-C. Chen, S.-L. Chen, P. A. R. Abu, A high-accuracy and power-efficient self-optimizing wireless water level monitoring IOT device for smart city, *Sensors*, vol. 21, no. 6, 2021, pp. 1–18.
DOI: [10.3390/s21061936](https://doi.org/10.3390/s21061936)
 - [20] P. Mayer, M. Magno, A. Berger, L. Benini, RTK-LoRa: High-precision, long-range, and energy-efficient localization for mobile IoT devices, *IEEE Transactions on Instrumentation and Measurement*, vol. 70, 2021, no. 3000611.
DOI: [10.1109/TIM.2020.3042296](https://doi.org/10.1109/TIM.2020.3042296)
 - [21] Li Lei, Zhang He Sheng, Liu Xuan, Development of low power consumption manhole cover monitoring device using LoRa, IEEE Int. Instrumentation and Measurement Technology Conf. I2MTC, Auckland, New Zealand, 20-23 May. 2019.
DOI: [10.1109/I2MTC.2019.8826885](https://doi.org/10.1109/I2MTC.2019.8826885)
 - [22] A. Q. Tameemi, Reliable battery terminal voltage collapse detection using supervised machine learning approaches, *IEEE Sensors Journal*, vol. 22, no. 1, 2022, pp. 795–802.
DOI: [10.1109/JSEN.2021.3131859](https://doi.org/10.1109/JSEN.2021.3131859)
 - [23] B. Rente, M. Fabian, M. Vidakovic, X. Liu, X. Li, K. Li, T. Sun, K. T. V. Grattan, Lithium-ion battery state-of-charge estimator based on FBG-based strain sensor and employing machine learning, *IEEE Sensors Journal*, vol. 21, no. 2, 2021, pp. 1453–1460.
DOI: [10.1109/JSEN.2020.3016080](https://doi.org/10.1109/JSEN.2020.3016080)
 - [24] Z. Ni, Y. Yang, A combined data-model method for state of charge estimation of lithium-ion batteries, *IEEE Transactions on Instrumentation and Measurement*, 2021, no. 2503611.
DOI: [10.1109/TIM.2021.3137550](https://doi.org/10.1109/TIM.2021.3137550)
 - [25] S. S. Afshari, S. Cui, X. Xu, X. Liang, Remaining useful life early prediction of batteries based on the differential voltage and differential capacity curves, *IEEE Transactions on Instrumentation and Measurement*, 2021, no. 6500709.
DOI: [10.1109/TIM.2021.3117631](https://doi.org/10.1109/TIM.2021.3117631)
 - [26] Y. Li, H. Sheng, Y. Cheng, H. Kuang, Lithium-ion battery state of health monitoring based on ensemble learning, IEEE Int. Instrumentation and Measurement Technology Conf. I2MTC, Auckland, New Zealand, 20-23 May. 2019.
DOI: [doi: 10.1109/I2MTC.2019.8826824](https://doi.org/10.1109/I2MTC.2019.8826824)
 - [27] B. Saha, K. Goebel, S. Poll, J. Christophersen, Prognostics methods for battery health monitoring using a bayesian framework, *IEEE Transactions on Instrumentation and Measurement*, vol. 58, no. 2, 2009, pp. 291–296.
DOI: [10.1109/TIM.2008.2005965](https://doi.org/10.1109/TIM.2008.2005965)
 - [28] Tinovi, tinovi.com. Online [Accessed 21 March 2023]
<https://tinovi.com/shop/lorawan-soil-moisture-temperature-air-temperature-humidity-12v-output-from-battery>
 - [29] A. Hills, N. Hampson, The Li-SOCl₂ cell—a review, *Journal of power sources*, vol. 24, no. 4, 1988, pp. 253–271.
DOI: [10.1016/0378-7753\(88\)80102-2](https://doi.org/10.1016/0378-7753(88)80102-2)
 - [30] E. S. Takeuchi, S. M. Meyer, C. F. Holmes, Assessment of capacity loss in low-rate lithium/bromine chloride in thionyl chloride cells by microcalorimetry and long-term discharge, *Journal of The Electrochemical Society*, vol. 137, no. 6, 1990, pp. 1665–1670.
DOI: [10.1149/1.2086768](https://doi.org/10.1149/1.2086768)
 - [31] “SAFT LS 17500 Lithium Thionyl Chloride primary cell”
<https://docs.rs-online.com/0d06/0900766b8017f0a9.pdf>.
 - [32] Y. Gong, X. Zhang, H. Li, H. Liao, Z. Meng, Y. Liu, Z. Huang, Estimation of Peukert Constant of Lithium-ion Batteries and its Application in Battery Discharging Time Prediction, 2020 IEEE Energy Conversion Congress and Exposition (ECCE), Detroit, MI, USA, 11-15 October 2020, pp. 905–910.
DOI: [10.1109/ECCE44975.2020.9236241](https://doi.org/10.1109/ECCE44975.2020.9236241)
 - [33] O. Tremblay, L.-A. Dessaint, Experimental validation of a battery dynamic model for EV applications, *World Electric Vehicle Journal*, vol. 3, no. 2, 2009, pp. 289–298.
DOI: [10.3390/wevj3020289](https://doi.org/10.3390/wevj3020289)
 - [34] G. Dong, X. Zhang, C. Zhang, Z. Chen, A method for state of energy estimation of lithium-ion batteries based on neural network model, *Energy*, vol. 90, Oct. 2015, pp. 879–888.
DOI: [10.1016/j.energy.2015.07.120](https://doi.org/10.1016/j.energy.2015.07.120)
 - [35] M. Charkhgard, M. Farrokhi, State-of-Charge Estimation for Lithium-Ion Batteries Using Neural Networks and EKF, *IEEE Transactions on Industrial Electronics*, vol. 57, no. 12, December 2010, pp. 4178–4187.
DOI: [10.1109/TIE.2010.2043035](https://doi.org/10.1109/TIE.2010.2043035)
 - [36] L. Kang, X. Zhao, J. Ma, A new neural network model for the state-of-charge estimation in the battery degradation process, *Applied Energy*, vol. 121, May 2014, pp. 20–27.
DOI: [10.1016/j.apenergy.2014.01.066](https://doi.org/10.1016/j.apenergy.2014.01.066).